THE JOURNAL OF BIOLOGICAL CHEMISTRY
Vol. 276, No. 28, Issue of July 13, pp. 26154–26163, 2001

Printed in U.S.A.

Crystal Structure of *Bacillus subtilis* Isocitrate Dehydrogenase at 1.55 Å

INSIGHTS INTO THE NATURE OF SUBSTRATE SPECIFICITY EXHIBITED BY *ESCHERICHIA COLI* ISOCITRATE DEHYDROGENASE KINASE/PHOSPHATASE*

Received for publication, February 7, 2001, and in revised form, March 29, 2001
Published, JBC Papers in Press, April 4, 2001, DOI 10.1074/jbc.M101191200

Satinder K. Singh‡, Kiyoshi Matsuno§¶, David C. LaPorte‡, and Leonard J. Banaszak‡‖

From the ‡Department of Biochemistry, Molecular Biology, and Biophysics, University of Minnesota, Minneapolis, Minnesota 55455 and the §Department of Molecular Biology and Microbiology, Tufts University School of Medicine, Boston, Massachusetts 02111

Isocitrate dehydrogenase from *Bacillus subtilis* (BsIDH) is a member of a family of metal-dependent decarboxylating dehydrogenases. Its crystal structure was solved to 1.55 Å and detailed comparisons with the homologue from *Escherichia coli* (EcIDH), the founding member of this family, were made. Although the two IDHs are structurally similar, there are three notable differences between them. First, a mostly nonpolar β-strand and two connecting loops in the small domain of EcIDH are replaced by two polar α-helices in BsIDH. Because of a 13-residue insert in this region of BsIDH, these helices protrude over the active site cleft of the opposing monomer. Second, a coil leading into this cleft, the so-called "phosphorylation" loop, is bent inward in the *B. subtilis* enzyme, narrowing the entrance to the active site from about 12 to 4 Å. Third, although BsIDH is a homodimer, the two unique crystallographic subunits of BsIDH are not structurally identical. The two monomers appear to differ by a domain shift of the large domain relative to the small domain/clasp region, reminiscent of what has been observed in the open/closed conformations of EcIDH. In *Escherichia coli*, IDH is regulated by reversible phosphorylation by the bifunctional enzyme IDH kinase/phosphatase (IDH-K/P). The site of phosphorylation is Ser^{113}, which lies deep within the active site crevice. Structural differences between EcIDH and BsIDH may explain disparities in their abilities to act as substrates for IDH-K/P.

Isocitrate dehydrogenase (EC 1.1.1.42) from *Escherichia coli* (EcIDH)[1] is a homodimeric enzyme that catalyzes the oxidative decarboxylation of isocitrate to yield α-ketoglutarate and CO_2 with concomitant reduction of $NADP^+$ to NADPH (1). It lies at a critical juncture between the Krebs cycle and the glyoxylate bypass, a pathway required for growth on substrates such as acetate, ethanol, or fatty acids. When one of these substrates serves as the sole source of carbon, induction of the two glyoxylate enzymes, isocitrate lyase and malate synthase, is required to circumvent the quantitative loss of CO_2 in the Krebs cycle (2). Under these nutritional conditions, ~75% of the EcIDH is completely inactivated by phosphorylation, thereby partitioning most of the isocitrate through the glyoxylate shunt (3–5).

Phosphorylation of EcIDH occurs on an active site serine (Ser^{113}) and involves only minor movements among some neighboring residues (6). No long-range conformational changes are triggered, unlike what is observed for enzymes typified by glycogen phosphorylase (7, 8). In the active, dephosphorylated enzyme, isocitrate is hydrogen-bonded to the γ-hydroxyl of Ser^{113} (9–11). Phosphorylation of EcIDH prevents isocitrate binding by eliminating this hydrogen bond and by introducing a source of electrostatic repulsion (9, 12, 13) and steric hindrance (14) with the γ-carboxylate of isocitrate.

The addition and removal of the phosphate group are catalyzed by a bifunctional 136-kDa dimer, isocitrate dehydrogenase kinase/phosphatase (IDH-K/P) (15). Although the mechanism by which phosphorylation inactivates EcIDH has been elucidated, the nature of the protein-protein interactions between EcIDH and its kinase/phosphatase has yet to be determined. The interface between these two enzymes must be extensive since IDH-K/P, in stark contrast to cAMP-dependent protein kinase (16, 17), can phosphorylate neither proteolytic fragments derived from EcIDH nor a synthetic peptide corresponding to the sequence around the phosphorylation site[2] (18). In addition, mutations within the $NADP^+$ binding site, specifically the adenosine 2′,5′-diphosphate binding site, which is fully 13 Å away from the target serine, decrease the K_m of IDH kinase for EcIDH by 10-fold (19).

In EcIDH, the target serine is sequestered in an interdomain cleft between the two monomers (20). How then does IDH-K/P access the serine? A plausible hypothesis serendipitously emerged with the structure of an orthorhombic, "open" crystal form of EcIDH, where a 16° domain rotation had widened the entrance to the active site cavity from 5 to 13 Å (21). A model was proposed in which EcIDH exists in a conformational equi-

* This research was supported by a Howard Hughes Medical Institute Predoctoral Fellowship (to S. K. S.), National Science Foundation Research Grant MCB-96036569 (to L. J. B.), and National Institutes of Health Research Grant GM 36718 to Dr. Abraham L. Sonenshein (former postdoctoral advisor of K. M.). Use of the Argonne National Laboratory Structural Biology Center beamlines at the Advanced Photon Source was supported by the U.S. Department of Energy, Office of Biological and Environmental Research under Contract No. W-31-109-ENG-38. The costs of publication of this article were defrayed in part by the payment of page charges. This article must therefore be hereby marked "*advertisement*" in accordance with 18 U.S.C. Section 1734 solely to indicate this fact.

¶ Present address: Ajinomoto Co., Inc., Fermentation and Biotechnology Laboratories, 1-1 Suzuki, Kawasaki, Kanagawa, Japan 210-8681.

‖ To whom correspondence should be addressed: Dept. of Biochemistry, Molecular Biology, and Biophysics, 6-155 Jackson Hall, 321 Church St. S.E., Minneapolis, MN 55455. Tel.: 612-626-6597; Fax: 612-624-5121; E-mail: len_b@dcmir.med.umn.edu.

[1] The abbreviations used are: EcIDH, isocitrate dehydrogenase from *E. coli*; BsIDH, isocitrate dehydrogenase from *B. subtilis*; IDH-K/P, isocitrate dehydrogenase kinase/phosphatase; βME, β-mercaptoethanol; MOPS, 4-morpholinepropanesulfonic acid; PEG, polyethylene glycol; r.m.s., root mean square.

[2] S. P. Miller, R. Chen, E. J. Karschnia, C. Romfo, A. M. Dean, and D. C. LaPorte, unpublished observation.

librium between open and closed states, with IDH-K/P being able to phosphorylate Ser^{113} only in the open form. Closer inspection of the model also revealed that the domain rotation had disrupted the substrate binding site by moving apart the amino acids responsible for forming this site. From this observation, it was further postulated that the substrates of EcIDH, isocitrate and $NADP^+$, control the phosphorylation cycle by shifting EcIDH into the closed conformation, thereby precluding IDH-K/P from accessing the sequestered serine (21). Despite the apparent flexibility of EcIDH, it was acknowledged that additional conformational changes, perhaps induced by the binding of IDH-K/P, would be required for Ser^{113} to become more fully solvent-exposed (21).

We have addressed the question of accessibility by more closely examining the substrate specificity of IDH-K/P. We chose to study a homologue of EcIDH, isocitrate dehydrogenase from *Bacillus subtilis* (BsIDH), and found that it is an extremely poor substrate of both the kinase and phosphatase.[3] This was an unexpected finding since BsIDH is 67% identical to its *E. coli* counterpart and is 100% identical in primary sequence around the phosphorylation site. Furthermore, it exhibits almost complete conservation of active site amino acids (see Fig. 1). It should be noted that there is no evidence that BsIDH is phosphorylated *in vivo*.[4] Because of initial kinetic data demonstrating a large disparity between the abilities of EcIDH and BsIDH to serve as substrates for IDH-K/P, a structural comparison between these two IDHs became an immediate goal. This report describes the results of that pursuit in the 1.55-Å crystal structure of BsIDH.

EXPERIMENTAL PROCEDURES

Expression and Purification of BsIDH—The gene encoding BsIDH (*citC*) was obtained from an *Xba*I-*Xho*I fragment of pKM11 (22) and subcloned into an *Xba*I + *Xho*I-cut pET16b (Novagen) vector, under control of the T7 promoter, to generate pKM14 for overexpression in *E. coli*. The lysogenic *E. coli* host strain (KME44 [KKL1{λDE3}]), in turn, contained a chromosomal copy of the T7 RNA polymerase gene under *lacUV5* control. To prevent contamination from endogenous EcIDH, the strain was specifically designed to possess a kanamycin resistance cassette (kan^R) in place of *icd*, the gene encoding EcIDH.

After pKM14 had been transformed into KME44, a single colony was used to inoculate 15 ml of LBG medium (1% Tryptone, 1% NaCl, 0.5% yeast extract, 0.2% glucose, 50 μg/ml amp, and 10 μg/ml kan) and grown overnight. The next morning, 1 liter of fresh LBG was inoculated with 10 ml of the preculture and grown at 37 °C in a gyrating incubator until the A_{600} reached 0.4–0.5. At this point, expression of *citC* was induced with 0.5 mM isopropyl-β-D-thiogalactoside, and the cells were allowed to grow for an additional 3–4 h. Bacteria were harvested by centrifuging at 4500 × *g* for 10 min, washed with buffer I (20 mM Tris-HCl (pH 7.4), 1 mM citrate, 5 mM $MgCl_2$, 5 mM β-mercaptoethanol (βME), 0.5 mM phenylmethylsulfonyl fluoride, 10% glycerol), and resuspended in 20 ml of the same buffer.

All manipulations henceforth described occurred either at 4 °C or on ice. The cells were disrupted by sonication and centrifuged at 27,000 × *g* for 20 min to remove cell debris, after which the crude extract was subjected to two ammonium sulfate fractionations: 45% and then 85%. BsIDH precipitated at 85% saturation. Following centrifugation at 27,000 × *g* for 20 min, the pellet was resuspended in 20 ml of buffer I and dialyzed against three 500-ml changes of the same buffer. A 50% solution of polyethylene glycol 8000 (PEG 8K) was subsequently added to the sample in two steps (first to 8%, then to 18%), and the mixture was then centrifuged at 15,000 × *g* for 20 min.

The resulting pellet was resuspended in 20 ml of buffer I and applied to a DEAE-Sephacel column (1.5 × 20 cm, 35 ml, Sigma Chemical Co.) that had been pre-equilibrated with 100 ml of 0.5 M Tris-HCl (pH 7.4) and 100 ml of buffer I. The column was washed with 100 ml of buffer I containing 100 mM NaCl before eluting BsIDH with a linear gradient of 100–250 mM NaCl (150 ml). The pooled fractions were then dialyzed against two 1-liter changes of buffer I, centrifuged, and applied to a pre-equilibrated Affi-Gel Blue (100–200 mesh, Bio-Rad) column (1 × 9 cm, 7.5 ml). BsIDH was eluted with a linear gradient of 0–300 mM NaCl (150 ml), dialyzed against buffer I, and concentrated to 7–8 mg/ml with a Centricon 10 ultrafiltration apparatus. Purification was monitored throughout the procedure by both isocitrate dehydrogenase assays (see below) and A_{280} readings. Final protein concentrations were calculated by the Peterson protocol (23), a variation of the Lowry method (24), using bovine serum albumin as the standard. BsIDH was >98% pure, as judged by SDS-polyacrylamide gel electrophoresis followed by Coomassie Blue staining (data not shown). Typically, 1 liter of cells yielded 20 mg of pure protein.

TABLE I
Data collection statistics

X-ray wavelength (Å)	1.0332
Space group	$P2_1$
Cell dimensions	
a (Å)	73.7
b (Å)	73.3
c (Å)	80.9
β (degrees)	109
Molecules/asymmetric unit	2
Observations	244,629
Unique reflections	114,797
Redundancy	2.13
R_{merge} (%)[a]	7.7
Maximum resolution (Å)	1.50
Completeness (%)	
Overall	88.5
to 1.50 Å	46.6
to 1.69 Å	99.8
to 1.78 Å	100.

[a] $R_{merge} = \Sigma_{hkl}\Sigma_i|I_i(hkl)_i - \langle I(hkl)\rangle|/\Sigma_{hkl}\Sigma_i I_i(hkl)$.

Dehydrogenase Assays—BsIDH activities were determined spectrophotometrically by measuring the reduction of $NADP^+$ to NADPH at 340 nm. The reaction mixture (1 ml) contained 25 mM MOPS (pH 7.5), 2.5 mM $NADP^+$, 0.50 mM D,L-isocitrate, and 5 mM $MgCl_2$. Reactions were initiated by the addition of 10 μl of each column fraction or appropriate dilution thereof. The rate was calculated as ΔA_{340}/min, with an extinction coefficient of 6220 M^{-1} cm^{-1} for NADPH and a path length of 1 cm.

Crystallization of BsIDH—Promising crystallization trials were conducted at 18 °C via hanging drop vapor diffusion in 100 mM citrate buffer (pH 4.8–5.0). Polyethylene glycol 4000 (PEG 4K) was used as the precipitant. Although needle-like crystals grew almost instantaneously, they diffracted to only 4 Å. To reduce the rate of growth, the concentration of PEG 4K was decreased from 30–35% and varying amounts (15–25%) of propylene glycol were added. Rod-shaped crystals (0.8 × 0.3 × 0.2 mm) that consistently diffracted to 2.1–2.5 Å grew within 3 days of standing *versus* a solution of 100 mM citrate (pH 4.9), 18–23% polyethylene glycol 4000, and 17–20% propylene glycol. The optimal crystals formed in a drop containing 3 μl of protein (7.9 mg/ml) and 3 μl of mother liquor (100 mM citrate (pH 4.9), 23% PEG 4K, 18% propylene glycol).

BsIDH crystals belonged to the monoclinic space group $P2_1$ and had the following unit cell dimensions: a = 73.7 Å, b = 73.3 Å, c = 80.9 Å, α = γ = 90°, β = 109°. The presence of a screw axis was confirmed by examining pseudoprecession images and locating systematic absences along *k* in both 0kl and hk0 zones. A Matthews' coefficient (25), V_m, of 2.4 $Å^3$/Da correlated with the presence of two monomers per asymmetric unit.

X-ray Diffraction Studies—Initial diffraction data were collected at room temperature on a Siemens multiwire area detector using monochromated CuK_α radiation generated from a Rigaku RU-200B rotating anode. Processing of raw data was completed with the XENGEN software package (26). X-ray intensities employed for final structure determination were measured at 110 K on a 3 × 3 charge-coupled device area detector using synchrotron radiation at a wavelength of 1.0332 Å on beamline 19-ID of the Advanced Photon Source (Structural Biology Center-CAT; Argonne National Laboratory). The single crystal diffracted to 1.50 Å, and the data are 99.8% complete to 1.69 Å. A total of 244,629 observations and 114,797 unique reflections between 99.0 and 1.50 Å were integrated with the program DENZO and scaled with SCALEPACK (27). Statistics are summarized in Table I.

Structure Determination—Despite the predicted presence of two subunits within the asymmetric unit, a self-rotation function (28, 29)

[3] S. K. Singh, S. P. Miller, L. J. Banaszak, and D. C. LaPorte, manuscript in preparation.

[4] A. L. Sonenshein, personal communication.

resulted in only a small, seemingly inconsequential peak at $\varphi = 90°$, $\phi = 35°$, and $\kappa = 165°$. It was originally assumed, therefore, that the orientation of the two monomers was approximately parallel to the 2-fold screw axis.

Initial phases for BsIDH were determined by molecular replacement, as implemented in X-PLOR (30), employing the monomer form of EcIDH (20; Protein Data Bank code 3ICD) as a search probe. To more closely mimic the *B. subtilis* enzyme, the following alterations were made to the EcIDH coordinate file after solvent molecules had been removed: 1) the first seven amino acids were deleted since they do not exist in BsIDH; 2) amino acids with similar chemical and/or structural properties in both enzymes (*e.g.* tyrosine in EcIDH, phenylalanine in BsIDH) were exchanged; and 3) all other nonidentical residues were converted to alanine. A cross-rotation search (28, 29) with the modified probe and subsequent Patterson correlation refinement (31) from 10 to 4 Å produced two peaks whose positions were related by the spherical coordinates indicated in the self-rotation function described above. Both of these solutions scored ~7σ above the mean and 2.5σ above the next highest peak. These peaks were treated as the two monomers (A and B) of the BsIDH dimer. After one subunit was located by the first translation search (32), utilizing data from 10 to 4 Å, its position was fixed while the position of the second subunit was ascertained.

Model Building and Refinement—Rigid-body refinement in X-PLOR (30) was attempted to optimize the molecular replacement solution using data from 8 to 3 Å and an F/σ amplitude cutoff of 2.0. However, it raised the crystallographic R-factor (R_{cryst}) (33) from 44.4% to 51.1%. Analysis of the calculation revealed that the starting van der Waals energy levels were extraordinarily high, suggesting that some atoms in the model were too close. To relieve this strain, an energy level minimization procedure was invoked instead. This reduced R_{cryst} from 44.4% to 40.0% and R_{free} (34) from 43.9% to 42.5%. Five percent of the reflections were removed for the test set.

A simulated annealing run (35) using data from 8 to 2.5 Å and an F/σ amplitude cutoff of 2.0 caused a precipitous drop in R_{cryst} (to 31.8%) but only a modest improvement in R_{free} (to 41.7%). A plot of R_{cryst} and R_{free} in the resolution range of 8 to 3 Å demonstrated that most of the error was centered on the lower resolution data. This and close inspection of theoretical Luzzati plots (36) pointed to the need for bulk solvent correction (37). Once applied, R_{cryst} and R_{free} fell to 30.2% and 39.5%, respectively, for data between 20 and 2.5 Å. A single round of positional and individual B-factor refinement, as implemented in X-PLOR (30), further reduced these values to 26.2% and 37.8%.

Model building was performed with the graphics program O (38). Initial $2|F_o| - |F_c|$ maps contoured at 1σ and incorporating data from 20 to 2.5 Å displayed fairly well-defined electron density for both monomers in the asymmetric unit with the following exceptions. First, amino acids Leu^{94}-Ile^{102} (Leu^{103}-Ile^{111} in EcIDH), part of the loop between β-strand C and α-helix d (Figs. 1 and 2), were disordered in monomer B, although they resided in contiguous density in monomer A. The significance of this apparent discrepancy is addressed under "Results and Discussion" below. Second, there was no definitive density for the N-terminal methionine or for residues 72–75, 241–275, and 333–340 in either monomer. In fact, strong negative density (−8σ) was covering these latter three areas in a $|F_o| - |F_c|$ map contoured at 3σ. These segments correspond, respectively, to a 2-amino acid deletion (in and after α-helix b), a 13-amino acid insertion (middle part of α-helices g2/g3), and a two-amino acid insertion (between β-strands D and E) in the BsIDH sequence (see Fig. 1). Residues 72–75 (80–84 in EcIDH), 241–275 (250–271 in EcIDH), and 333–340 (329–334 in EcIDH) were consequently removed from the model until positive density could be discerned in future $|F_o| - |F_c|$ maps. An attempt to apply noncrystallographic symmetry restraints early in refinement resulted in slight increases in both R_{cryst} and R_{free}. Therefore, the monomers were refined independently.

At this juncture, because of difficulties encountered with modeling residues 241–275, including the 13-amino acid insert, data to 1.55 Å with an F/σ amplitude cutoff of 0.0 were incorporated in one step rather than incrementally. This, not surprisingly, raised R_{cryst} and R_{free} to 45.3% and 47.9%, respectively, from their previous values of 25.2% and 35.7%. Nevertheless, a round of Powell minimization, simulated annealing, positional, and individual B-factor refinement against bulk-solvent-corrected data decreased those figures to 31.1% and 35.1%. Despite the inclusion of all data, however, amino acids 241–275 remained in broken density in both subunits. The noncrystallographic symmetry operator was thus employed to generate averaged $2|F_o| - |F_c|$ maps employing the MAMA (39, 40) and AVE protocols (41). For both monomers, this resulted in contiguous density for 2–3 residues on either side of the 35-residue gap. The program MAID (42) was then used to construct 4–6 amino acids per modeling session, and after subsequent reciprocal-space refinement in X-PLOR against bulk-solvent-corrected data, unaveraged maps were utilized to more precisely position these residues. This iterative process continued until all 70 amino acids (35 in each subunit) were properly built into $2|F_o| - |F_c|$ maps (contoured at 1σ) and until no negative or positive peaks remained in $|F_o| - |F_c|$ maps (contoured at 3σ). Each round of model building and refinement reduced R_{cryst} and R_{free}, yielding more readily interpretable electron density.

Solvent molecules were added to the model when R_{cryst} fell below 28.0%. Placement was aided by the use of a density peak search algorithm in O. Waters were kept only if they met the following criteria: 1) they were present in both $2|F_o| - |F_c|$ maps contoured at 1σ and $|F_o| - |F_c|$ maps contoured at 3σ; 2) they were 2.5–3.6 Å away from a suitable hydrogen bond donor/acceptor atom; and 3) their temperature factors did not rise above 60 Å^2 during subsequent refinement.

Stereochemical quality of the model was assessed with the program PROCHECK (43). Comparisons between the two subunits of BsIDH and between BsIDH and the various crystal structures of EcIDH were accomplished with a least-squares approach as implemented in O (38) and LSQMAN (44) and graphically depicted with Kaleidagraph 3.5 Synergy software (45). Molecular surface calculations were completed with GRASP (46), and structure figures were prepared with SETOR (47) except where noted. Atomic coordinates and structure factors have been deposited in the Protein Data Bank under accession code 1HQS.

RESULTS AND DISCUSSION

Model and Electron Density Map—Final cycles of reciprocal-space refinement were completed with alternate rounds of Powell minimization and individual B-factor scaling. By this point, R_{cryst} and R_{free} were 22.7% and 28.1%, respectively, and 417 out of 423 side chain atoms were in place. However, there were still several regions of unexplained electron density. The first region focused on seven distinct +6σ features positioned throughout the protein, all of which were interpreted as molecules of propylene glycol (ligand numbers 901–907), a constituent of the crystallization medium. The second region, a series of +8σ peaks corresponding to 4 atoms at the tip of Cys^{118} in both subunits, appears to have resulted from these residues being modified by β-mercaptoethanol (βME), the reducing agent employed during protein purification. (They are designated as CME in the coordinate file instead of CYS to distinguish them from normal -SH cysteines). Note that Cys^{118} is an active site residue. Nevertheless, as discussed below, the catalytic residues of BsIDH and EcIDH are virtually superimposable. Moreover, prolonged incubation of BsIDH with βME had no detectable effect on IDH activity (data not shown). Taken together, these data indicate that the modification did not drastically perturb the structure.

Additional electron density (+6σ to +9σ in $|F_o| - |F_c|$ maps) was observed in both active sites, although it was of much stronger intensity and more clearly defined in monomer A. Here, the density was branched and large enough to include 13 atoms. It resembled citrate (ligand number 425) and was modeled as such. The density in monomer B, on the other hand, was only large enough to include six atoms but was modeled as a citrate molecule (ligand number 825). Upon placement and subsequent refinement, $2|F_o| - |F_c|$ density for 10 of 13 atoms appeared. A small negative peak (−3.4σ) on atoms O5 and C6, however, later forced them to be refined with zero occupancy. This, along with a slight increase in thermal factors, suggests that the citrate molecule may not have been bound as tightly in monomer B as in monomer A.

Placement of the citrate and propylene glycol, as well as assignment of alternate conformations for 28 residues, decreased R_{cryst} and R_{free} to their final values of 20.2 and 24.9%, respectively, for all data between 20.0 and 1.55 Å. The final model of BsIDH includes 846/846 amino acids, 608 waters, 7 molecules of propylene glycol, and 2 molecules of citrate. The crystallographic asymmetric unit contains two monomers, between which the RMS deviation for all α-carbon atoms (423/

TABLE II
Residues with alternate conformations

Monomer A	Monomer B
A22 (isoleucine)	B11 (asparagine)
A84 (arginine)	B40 (lysine)
A111 (glutamine)	B95 (threonine)
A112 (glutamate)	B96 (threonine)
A113 (leucine)	B97 (proline)
A185 (serine)	B118 (cysteine modified with βME)
A214 (lysine)	B168 (serine)
A284 (serine)	B173 (glutamate)
A288 (isoleucine)	B225 (methionine)
A308 (leucine)	B247 (lysine)
A345 (histidine)	B284 (serine)
A346 (glycine)	B285 (isoleucine)
A365 (serine)	B291 (glutamine)
A388 (lysine)	
A403 (methionine)	

TABLE III
Refinement statistics

Estimated coordinate error = 0.20 Å.	
R_{cryst} (%)[a]	20.2
R_{free} (%)[b]	24.9
σ cutoff	0.0
Resolution range (Å)	20.0–1.55
Unique reflections used in refinement	109,218
Number of atoms in model	7445
Protein (includes atoms with alternate conformations)	6776
Water	608
Ligand	61
Number of residues with alternate conformations	28
Average *B*-factor (Å^2)	
Overall	23.1
Protein	22.0
Water	32.7
Ligand	43.7
r.m.s.d.[c] bond lengths (Å)	0.010
r.m.s.d. bond angles (degrees)	1.70
r.m.s.d. dihedral (degrees)	23.6
r.m.s.d. improper (degrees)	1.46
Ramachandran Geometry[d]	
Most favored (%)	90.5
Allowed (%)	8.2
Generously allowed (%)	0.8
Disallowed (%)	0.4
cis-Peptides (alternate conformation of Pro^{97} in monomer B)	1

[a] $R_{cryst} = \Sigma||F_{obs}|-|F_{calc}||/\Sigma|F_{obs}|$.
[b] An R_{free} test set of 5% of the total reflections was used.
[c] r.m.s.d., root mean square deviation.
[d] Ramachandran geometry was monitored using PROCHECK (43).

423) is 0.76 Å. The 28 amino acids with alternate conformations are noted in Table II. No attempt was made to refine the occupancies of these atoms, so each remains at 0.5. r.m.s. deviations for the structure fall within canonical values. Other crystallographic and model statistics are presented in Table III.

The electron density for the C terminus in both monomers is unequivocal. The second-to-last amino acid, Met^{422}, points into a hydrophobic pocket from the end of α-helix m and is stabilized by interactions with several residues (Val^{41}, Ala^{44}, Ala^{45}, Val^{382}, Leu^{418}, and Ile^{419}). The last amino acid in both subunits, Asp^{423}, is stabilized by the close juxtaposition of symmetry mates.

Unlike the C termini, the N termini remain somewhat disordered. The side chain of the first amino acid in monomer B, Met^{1}, could only be modeled in a $2|F_o| - |F_c|$ map contoured at 0.6σ. There is no visible electron density, even at this low contour level, for atoms beyond the β-carbon of Met^{1}, Gln^{3}, and Asn^{11} of monomer A. Hence, these side chains were generated in the graphics program O (39) using the most common rotamers, and their occupancies are set to 0.0 in the final list.

The model exhibits good stereochemistry with 90.5% of the amino acids in the most favored region of the Ramachandran diagram (48), although there are three outliers, Phe^{A87} (ϕ = 76.9°, φ = −49.6°), Phe^{B87} (ϕ = 70.6°, φ = −45.5°), and Thr^{A347} (ϕ = −7.1°, φ = −148.9°). The letters A and B are used to distinguish between the two subunits. The phenylalanines reside in unambiguous density, and in both subunits, the ring appears to cap α-helix c (Figs. 1 and 2). The turn at the end of this helix is very sharp, with the carbonyl oxygen of Tyr^{86} forming a hydrogen bond with the nitrogen of Ile^{88}. It is the form of this sharp turn that is responsible for the unusual ϕ and φ angles.

The unfavorable conformation of the third residue, Thr^{A347}, can be partially rationalized by the fact that its Oγ1 atom forms a hydrogen bond with its own backbone amide nitrogen. Its side chain resides in slightly disordered electron density. Disallowed $\phi\varphi$ angles are frequently found for the side chains of asparagine, serine, and threonine as a result of hydrogen bonds with the peptide nitrogen of the same residue. Curiously, the same residue in monomer B resides in excellent density and falls within the core α-region of the Ramachandran plot (ϕ = −75.0°, φ = −8.0°). It is stabilized by hydrogen bonds between its Oγ1 atom and its amide nitrogen, its carbonyl oxygen, and the amide nitrogen of Ala^{B348}.

Overall Structure of BsIDH—The tertiary structure of BsIDH (monomer A), along with associated secondary structural elements, is illustrated in Fig. 2, *panel A*. For comparison, the tertiary structure of EcIDH is depicted in *panel B*. The BsIDH dimer is shown in Fig. 3. The enzyme is topologically very similar to its *E. coli* counterpart (20), as was predicted by the extensive amino acid sequence homology (Fig. 1). Each subunit is composed of 13 β-strands and 15 α-helices rather than the 14 β-strands and 13 α-helices in EcIDH (20). Still, they are both divided into the same three distinct domains. The large domain falls into a general α + β classification and contains the N- and C-terminal segments, incorporating residues 1–115 and 322–423. A clasp domain encompasses residues 149–193 and is created only in the dimer, where constituent β-strands (M and N) and connecting α-helix e of each subunit interlock to form a hydrophobic core (Fig. 3*A*). The small domain adopts a parallel α/β conformation and contains residues 116–148 and 194–321, including the 13-amino acid insert. This insert and a number of the amino acids on either side (residues 251–276) form an α-helical motif (g2 and g3) that replaces β-strand K of EcIDH and the adjoining loops. β-Strand L has been shifted downstream by 3 amino acids and includes residues 248–250 (Figs. 1 and 2). It is this α-helical region (residues 246–276), emanating from the opposing monomer, that we propose to be a major obstacle for IDH-K/P (see below).

Dimerization Interface—The two monomers of BsIDH are related by a noncrystallographic dyad axis in contrast with EcIDH, whose subunits are related by a crystallographic 2-fold axis. For the most part, however, the intersubunit contacts are the same in both enzymes, mediated through expansive portions of the small and clasp domains. These include, but are not limited to, helices e, g1 (g in EcIDH), h, and i of monomer A and helices e, g1 (g in EcIDH), i, and h of monomer B. As expected, the buried solvent-accessible surface areas are comparable as well, with a 500-Å^2 greater buried surface in the BsIDH dimer than in the EcIDH dimer (3701 Å^2 *versus* 3206 Å^2). Thus, both enzymes form remarkably stable dimers.

Active Site—Comparison with EcIDH indicates that the active site of BsIDH is located in a cleft between the large and small domains and consists of residues from both subunits. Because citrate was found in the active site of both monomers,

FIG. 1. **Structure-based sequence alignment between BsIDH and EcIDH.** Identical residues are *light gray*, active site amino acids are *dark gray*, and the phosphorylated serine (also an active site residue) is *black*. Comparisons were made with the Mg^{2+}-isocitrate-EcIDH complex (9; PDB code 5ICD) because citrate was found in the active site of BsIDH. Note the *large white region* of dissimilarity (residues 246–276 in BsIDH, residues 255–272 in EcIDH), which includes a 13-amino acid insert in BsIDH. This region is demarcated with parentheses because of the lack of structural homology in this area. These amino acids were aligned according to an algorithm applied in LALNVIEW (49). Secondary structural assignments are indicated by the *bars* above the BsIDH sequence and below the EcIDH sequence. *Gray* and *black bars* designate β-strands and α-helices, respectively. To be consistent with assignments made in the original EcIDH structure (20; PDB code 3ICD), helices were labeled according to their order in the amino acid sequence, whereas strands were labeled according to their order (from *left* to *right*) in the two β-sheets (see Fig. 2), The *thinner*, *unlabeled bars* above the BsIDH sequence represent the four "extra" α-helices (residues 134–137, 148–153, 297–300, 348–352) and four "extra" β-strands (residues 8–10, 13–15, 394–395, 407–408) identified in BsIDH. Although these elements were not defined in the original structures of EcIDH (PDB codes 3ICD, 4ICD, 5ICD, and 9ICD), they are defined in more recent depositions (PDB codes 1AI2, 1BL5, and 1CW7).

FIG. 2. **Structural comparison between the BsIDH and EcIDH monomers.** *A*, a BsIDH monomer; *B*, an EcIDH monomer. In both panels, β-strands are *black* and α-helices are *gray*. Secondary structural assignments are indicated and correspond to the labels in the structure-based amino acid sequence alignment (Fig. 1). The serine targeted for phosphorylation (Ser^{104} in BsIDH, Ser^{113} in EcIDH) is represented by a *black dot*. Note the α-helical motif (*g2* and *g3*) in the small domain of BsIDH that replaces β-strand K and the two adjacent loops in EcIDH. This corresponds to the *white segment* of nonidentity in the alignment presented in Fig. 1. The three striped α-helical turns denote the 13-amino acid insert in BsIDH.

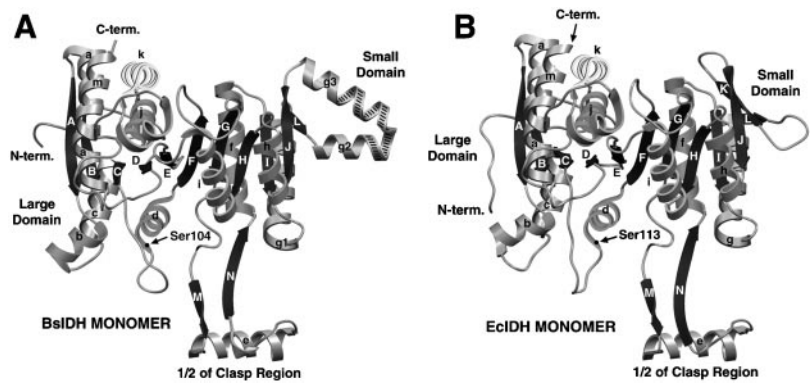

comparisons were made with the Mg^{2+}-isocitrate-EcIDH complex (9; PDB code 5ICD) rather than with the apo form (20; PDB code 3ICD). As is evident from Fig. 4*B*, those residues implicated in EcIDH as being essential for catalysis and substrate binding are structurally conserved in BsIDH. The citrate bound in the active site of BsIDH (Fig. 4*A*; omitted from Fig. 4*B* for clarity) is coordinated by some of the same amino acids as is Mg^{2+}-isocitrate in EcIDH (Table IV). This includes the serine phosphorylated by IDH-K/P (Ser^{104}, Fig. 4, *A* and *B*) whose γ-oxygen is 2.45 Å away from the O4 atom of citrate.

One exception to the similarity between the enzymes' active sites involves Arg^{A120} (Arg^{129} in EcIDH), which in BsIDH points upward, away from the citrate molecule (Fig. 4*B*). This shift may have been caused by the -S-CH_2-CH_2-OH moiety on Cys^{118}, but since βME does not affect BsIDH activity, the location of the Arg^{A120} side chain is probably not significant.

Another difference between the active sites of BsIDH and EcIDH involves Thr^{A96} (Thr^{105} in EcIDH). Although it is not a true active site amino acid, it forms part of a loop, the so-called "phosphorylation" loop (21), that leads into the active site. Its Oγ1 atom is 2.53 and 3.25 Å away from the O4 and O3 atoms, respectively, of citrate. The same atom in Thr^{105} of EcIDH is

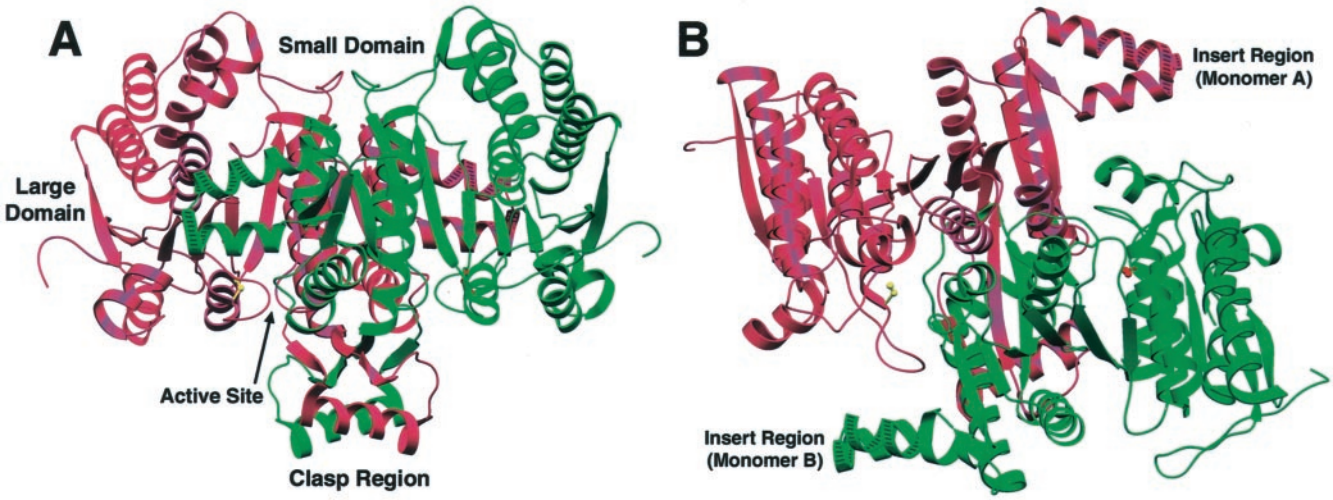

FIG. 3. **Cα trace of the BsIDH dimer (two perpendicular views).** Monomer A is *dark pink* and monomer B is *green*. *A*, the tertiary structure of BsIDH is very similar to that of the *E. coli* enzyme, each monomer possessing large, small, and clasp domains. The active site (one for each monomer) is indicated and is located in the cleft between the large and small domains. *B*, in this view, BsIDH has been rotated ~90° toward the reader with respect to the view in *panel A*. The *yellow* residue (*red* in the opposing monomer) is the serine targeted for phosphorylation (Ser^{104} in BsIDH, Ser^{113} in EcIDH). As in Fig. 2*A*, the three striped α-helical turns in the insert region of each subunit denote the 13-amino acid insert in BsIDH.

5.49 and 5.87 Å from the O4 and O3 atoms, respectively, of isocitrate. It is possible that the citrate influenced Thr^{A96} to assume this unusual position. This notion is bolstered by the presence of two conformers of Thr^{B96} in monomer B, only one of whose Oγ1 atom is within hydrogen-bonding distance of the O4 and O3 atoms of citrate. Recall that, in this subunit, citrate seems to be bound less tightly, as implied by its less well-defined electron density.

A final distinction between the active sites of BsIDH and EcIDH involves His^{345}. In monomer A of BsIDH, this residue adopts two alternate conformations (Fig. 4*A*). It exists in a single orientation in monomer B, pointing away from the bound citrate. His^{A345}, along with the neighboring Gly^{A346}, were modeled in two orientations to be consistent with imidazole ring density present on either side of the peptide backbone. Apparently, these two residues are highly mobile, "flipping" back and forth, toward and away from the bound citrate. The locations of the first conformer, His^{A345a}, as well as that of His^{B345}, match that of the homologous histidine (His^{339}) in EcIDH. However, in EcIDH, this amino acid adopts only a single conformation.

Aside from the minor variations outlined above, the active site architecture of both BsIDH and EcIDH is practically indistingishable. This conservation was expected since both enzymes catalyze the same reaction.

Heterogeneity between the Subunits of BsIDH—Although BsIDH is a homodimer, the structures of the individual monomers are not identical. This difference is apparent from the r.m.s. deviation, which is 0.76 Å for all α-carbon atoms (423/423). Nevertheless, even after considerable examination of the overlaid structures, no particular region could be pinpointed as the sole contributor of the disparity. We, therefore, suspected that the difference might have resulted from a conformational change similar to that observed for the orthorhombic ("open") form of EcIDH (21; PDB code 1SJS). The differences between the open/closed forms of EcIDH had been studied by breaking the monomer into its constituent domains and examining them via least square methods. A similar strategy was adopted here. For purposes of this analysis, the small domain and clasp region should be considered a single unit; the large domain is divided into two segments by the small/clasp domain.

The quantitative comparison of the BsIDH monomers is shown in Fig. 5*A*. The *solid line* depicts the results when the two subunits are overlaid using just the small/clasp domain; the *dotted line* is the graph that is generated when the two are superimposed with coordinates from just the large domain. Fig. 5*B* displays the results when analogous calculations are made with the closed and open forms of EcIDH. Both analyses are consistent with rotation of the large domain away from the small/clasp domain. The pivot points for this rotation can be determined from the intersections of the graphs. For EcIDH, this corresponds to the beginning/middle of β-strand F (amino acids Cys^{127}-Leu^{128}) and the beginning of β-stand E (amino acids Gly^{325}-Ala^{326}). For BsIDH, domain rotation corresponds to the end of α-helix d/the small loop before β-strand F (amino acids Gln^{111}-Leu^{115}) and the small loop preceding and including β-strand E (amino acids Gly^{325}-Asn^{333}). Intriguingly, the location of the pivot point approximately coincides with that observed in the open/closed forms of EcIDH.

Note from Fig. 5 that there is a relatively large disparity between the conformational differences in the two forms of EcIDH and the two crystalline subunits of BsIDH. The variability in coordinate distances range from 0.0 to 10.0 Å for EcIDH but only from 0.0 to 2.0 Å for BsIDH. The two monomers of BsIDH are from the same crystal structure, and the conformational differences appear to result only from relatively weak lattice packing phenomena, whereas those observed in EcIDH represent distinct conformational states. The correlation in conformational changes between the two proteins are, however, too similar to be a mere coincidence. Hence, both IDH molecules appear to be capable of varying degrees of domain rotation within a hinge region defined by β-strands E and F.

In the above assessment, a small domain shift seems to have occurred in monomer B. Additional support for this premise is suggested by a curious disparity between Thr^{95} to Ile^{102} in the two subunits. These residues comprise a majority of the loop, the "phosphorylation" loop, between β-strand C and α-helix d (Figs. 1 and 2). The stretch of 8 amino acids lies in unambiguous density in monomer A but is disordered in monomer B (Fig. 6). Three amino acids (Thr^{B95}, Thr^{B96}, Pro^{B97}) in monomer B have been modeled with alternate conformations to account for two areas of positive $|F_o| - |F_c|$ side chain density for Thr^{B95} and Thr^{B96}. Both *cis*- and *trans*-conformations were included for Pro^{B97} to accommodate the large range of motion putatively exhibited by Thr^{B96}. The present model produced the lowest

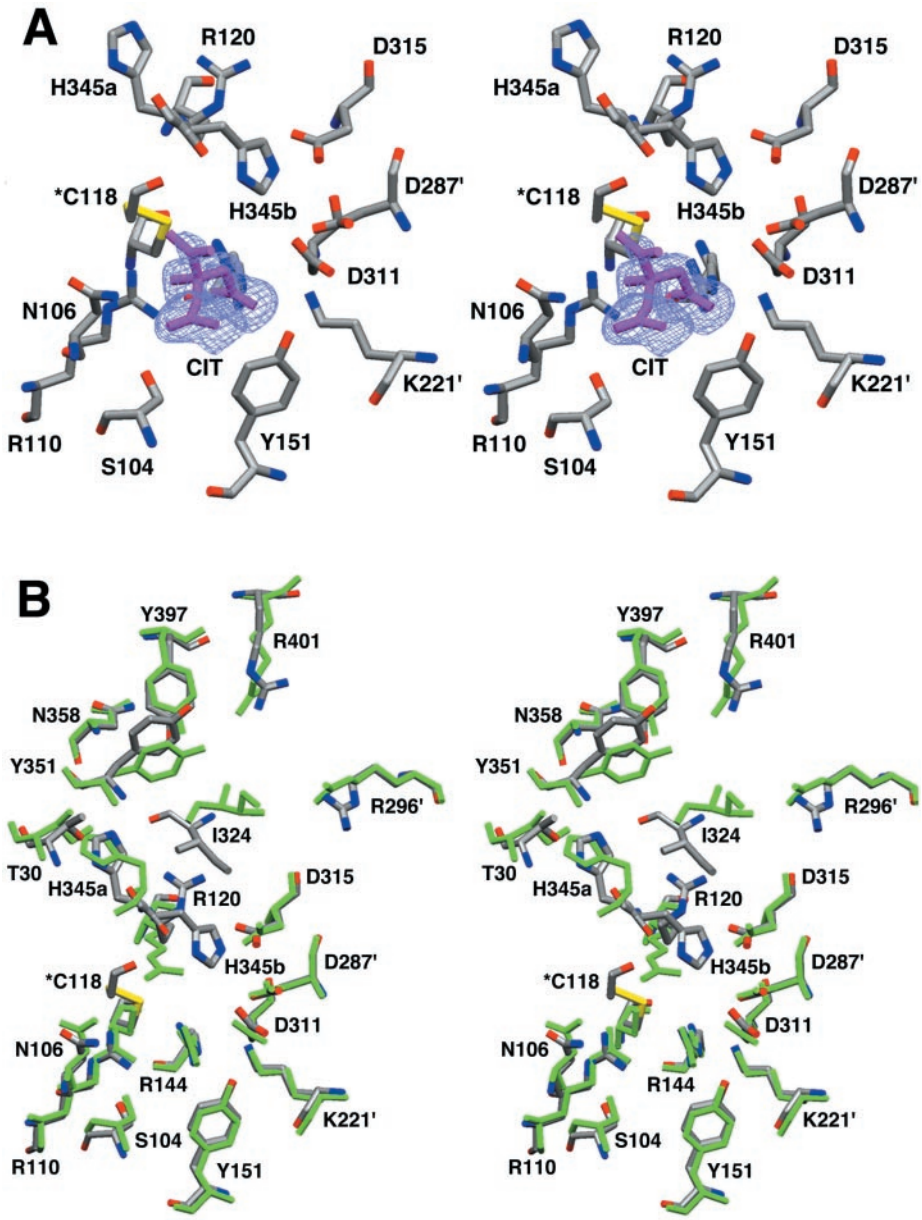

FIG. 4. **Active site of BsIDH and EcIDH.** *A*, divergent stereo diagram of the active site of BsIDH (monomer A) with bound citrate. Protein atoms are *multicolored*: *gray* (carbon), *red* (oxygen), *blue* (nitrogen), and *yellow* (sulfur). The apostrophe after *K221′* and *D287′* designate residues that emanate from the opposing monomer (subunit B). The *asterisk before C118* signifies that this amino acid has been modified by β-mercaptoethanol. The citrate molecule (*violet*) is shown in a lavender $2|F_o| - |F_c|$ map contoured at 1σ. *B*, divergent stereo diagram of the active site of EcIDH superimposed onto that of BsIDH. EcIDH residues are *light green*. BsIDH residues are colored as in *panel A*. Residue numbering is that of BsIDH. The equivalent amino acids in EcIDH, given in parentheses, are as follows: T30 (I37), S104 (S113), N106 (N115), R110 (R119), C118 (C127), R120 (R129), R144 (R153), Y151 (Y160), K221′ (K230′), D287′ (D283′), R296′ (R292′), D311 (D307), D315 (D311), I324 (I320), H345 (H339), Y351 (Y345), N358 (N352), Y397 (Y391), R401 (R395). Coordinates from the Mg^{2+}-isocitrate-EcIDH complex (9; PDB code 5ICD) were used for comparison because citrate was found in the active site of both monomers of BsIDH. Both citrate and Mg^{2+}-isocitrate (omitted from this image for clarity) are coordinated by many of the same residues, including the serine (Ser^{104} (Ser^{113} in EcIDH)) phosphorylated by IDH-K/P.

TABLE IV
Hydrogen bond pairs between citrate and BsIDH (monomer A)
Estimated coordinate error = 0.20 Å.

Hydrogen bond pair		Distance
		Å
CIT:O1	K221(B):NZ	2.97
CIT:O2	R110(A):NH1	2.75
	R110(A):NH2	3.22
	R144(A):NH1	2.93
CIT:O3	T96(A):OG1	3.25
CIT:O4	T96(A):OG1	2.53
	N106(A):ND2	2.72
	S104(A):OG	2.45
CIT:O5	None	
CIT:O6	None	
CIT:O7(OH)	R110(A):NH2	3.05
	R110(A):NH1	3.41

value for R_{free}. The fact that there are no crystal contacts stabilizing the loop in one subunit *versus* the other perhaps indicates that this loop is more mobile in monomer B than it is in monomer A. In a previous study describing the open form of EcIDH, it was reported that most of the homologous loop (Pro^{106}-Arg^{112}) was also disordered (21). This disorder was attributed to an increase in mobility that could possibly stabilize the open conformation. In BsIDH, as discussed above, only one of these loops is disordered, and it occurs in the subunit that has adopted a more open conformation, namely monomer B.

At this point, the physiological significance of the two conformational states in BsIDH remains unclear. Distinct conformational states have been observed in a number of enzymes, but these changes generally represent symmetrical movements of the entire protein. This contrasts with BsIDH, where the conformational states are represented by different subunits of the same crystal structure.

Properties of an Indented "Phosphorylation" Loop and the Insert Region of BsIDH—The structure of BsIDH was investigated in an attempt to understand the substrate specificity of IDH-K/P for EcIDH. BsIDH is a substrate for IDH-K/P, but the Michaelis constants for both the kinase and phosphatase are increased by over 50-fold.[3] The greatly reduced ability of BsIDH to serve as a substrate for *E. coli* IDH-K/P is consistent with the observation that BsIDH does not appear to be regulated by phosphorylation *in vivo*.[4] Understanding the struc-

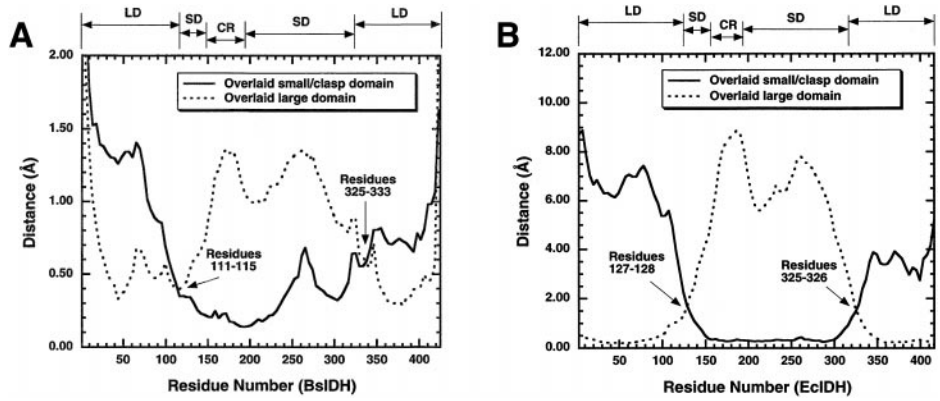

FIG. 5. **Graphical representation of domain movement in the two monomers of BsIDH and the open/closed forms of EcIDH.** A, BsIDH; *B*, EcIDH. Residue numbers are indicated. The relative displacements of equivalent Cα atoms are given in Å and represent distances after application of a "smoothing" function in Kaleidagraph (45). In both plots, the acronyms at the *top* refer to the domains of a monomer (*LD* = large domain, *SD* = small domain, *CR* = clasp region). The following protocol was used to generate the graphs. First, monomer A was rotated onto monomer B, aligning residues contained only in the large domain (amino acids 1–115 and 322–423). Distances between equivalent α-carbon atoms were then calculated and plotted *versus* residue number. Second, monomer A was rotated onto monomer B, aligning residues contained only in the small domain/clasp region (amino acids 116–321). Again, distances between equivalent α-carbon atoms were then calculated and plotted *versus* residue number. The two plots were subsequently combined to yield the single graph shown in *A*. The same procedure was subsequently performed for the open and closed forms of EcIDH to generate *B*.

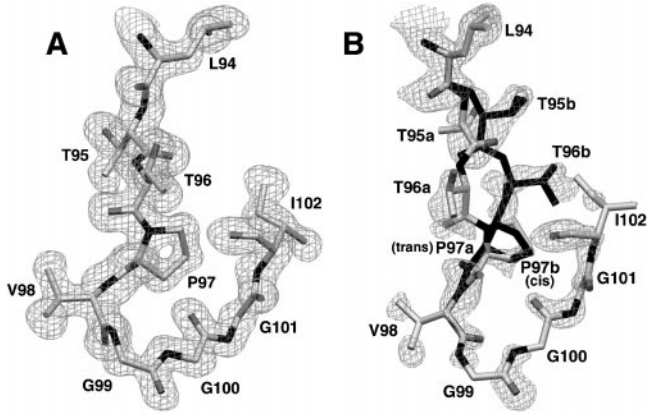

FIG. 6. **The phosphorylation loop is disordered in only one monomer of BsIDH.** $2|F_o| - |F_c|$ electron density maps, contoured at 1σ, of a majority of the phosphorylation loop in BsIDH. *A*, the loop in monomer A, illustrating the unequivocal position of the constituent amino acids; *B*, the loop in monomer B, depicting the ambiguous location, perhaps increased mobility, of the same residues. Atoms are shaded as follows: *light gray* (carbon), *dark gray* (oxygen), and *black* (nitrogen).

tural basis for the ability of IDH-K/P to distinguish between the two IDHs should provide insights into the substrate specificity of this regulatory enzyme.

The extreme disparity in the affinity of the two IDHs for IDH-K/P stands in striking contrast to the high degree of structural conservation between them (Figs. 2 and 7*A*). Indeed, the r.m.s. deviation between the dimers is 0.84 Å for 764 equivalent α-carbon atoms. Despite this congruence, there are two areas that exhibit noticeable departures in primary and secondary structure. These include the phosphorylation loop (the loop between β-strand C and α-helix d) and the insert region. They constitute the basis of three hypotheses that may explain why BsIDH is a poor substrate of the kinase/phosphatase.

One possible explanation revolves around diminished access to the phosphorylation site in BsIDH. The phosphorylation loop in both BsIDH and EcIDH is comprised of the same 11 amino acids (Pro^{93} to Arg^{103} (BsIDH numbering)). However, in BsIDH, this loop is indented or folded inward, narrowing the entrance to the active site from 11.9 to 4.1 Å (as measured from residues Gly^{A99} to Lys^{B226} (Gly^{108} to $Lys^{235'}$ in EcIDH)) (Fig. 7, *A* and *B*). There are no obvious crystal contacts forcing the loop to adopt this orientation, and the amino acids of the insert are too far to form hydrogen bonds or salt bridges (5–6 Å). Therefore, the positioning of this loop, composed of three contiguous glycines, might merely reflect the dramatic mobility of which it is capable.

Access to the phosphorylation site in BsIDH might also be restricted by the insert segment in the small domain. This region spans amino acids 246–276, which includes the 13-amino acid insert, and folds into a turn, a single β-strand (L) and two α-helices (g2 and g3). The analogous region in EcIDH is composed of a twisted antiparallel segment of β-sheet. This distinction is more evident in an overlay of the two dimers (Fig. 7*A*). The subdomain in BsIDH protrudes over the active site of the adjacent monomer, very possibly impeding IDH-K/P. The difference in steric hindrance that IDH-K/P might encounter as it attempts to phosphorylate/dephosphorylate EcIDH *versus* BsIDH is dramatically revealed in the surface rendering depicted in Fig. 7, *C* and *D*. It is clear from these illustrations that the phosphorylation site in the static BsIDH structure is more sequestered.

A second possible explanation for the reduced affinity of IDH-K/P for BsIDH focuses on an apparently reduced flexibility of the insert region. As shown in Fig. 7*B*, the residues in this insert are primarily polar, acidic, or basic, and as in most α-helices, their side chains point outward. However, these residues create a vast array of hydrogen bonds and salt bridges that may enhance the helices' rigidity. In contrast, the corresponding segment in EcIDH is an antiparallel β-hairpin that does not extend out as far. It is composed of mainly nonpolar amino acids, none of whose side chains form hydrogen bonds with each other and/or with the peptide backbone. Perhaps it is this lack of rigidity that enables IDH-K/P to "move" this section aside as it attempts to access the active site of IDH. Indeed, in the open form of EcIDH, a part of the corresponding region (the coil between β-strands K and L) no longer appears to shield the phosphorylation site as it does in the closed conformation (21).

A third possible explanation for the difference in the abilities of BsIDH and EcIDH to act as substrates for IDH-K/P proposes that the EcIDH subdomain that corresponds to the insert region in BsIDH serves as a docking site for IDH-K/P. Accordingly, a pre-catalytic complex forms between IDH and IDH-K/P, and this complex subsequently undergoes a conformational change that makes the phosphorylation site accessible to

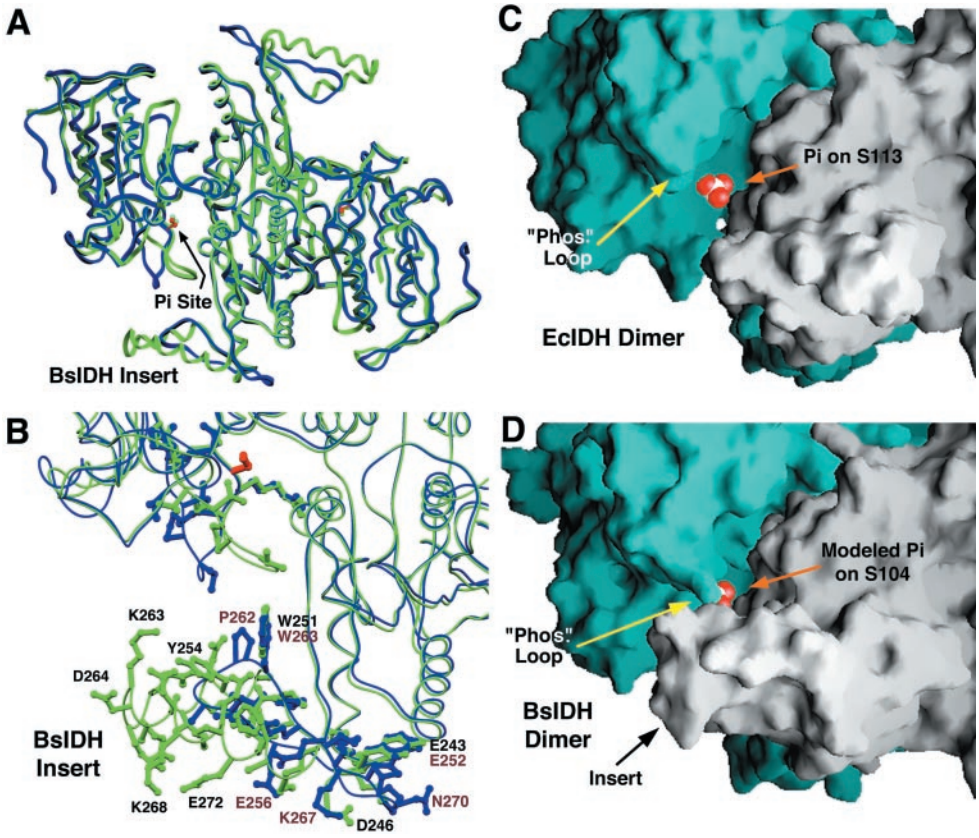

FIG. 7. **Accessibility of the phosphorylation site in BsIDH and EcIDH.** *A*, global overlay of the two IDHs. BsIDH is *light green* and EcIDH is *blue*. The phosphorylated serine (Ser^{104} in BsIDH, Ser^{113} in EcIDH) is *red*. *B*, magnification of the insert region and active site with relevant side chains added. Labels of selected residues in BsIDH are *black*; those in EcIDH are *reddish-gray*. The phosphorylated serine is *red* and is clearly occluded. Indicated amino acids in the insert region of BsIDH include ^{242}EKEYGDKVFTWAQYDRIAEEQGKDAANKAQSEAEAAGK^{278}. Indicated residues in this area of EcIDH include ^{251}REEFGGELIDGGPWLKVKNPNTGKE^{271}. Although there is little structural homology between the two IDHs in the insert region, there is a small stretch of β-strand that overlaps. The segment in BsIDH includes ^{247}KVFTWA^{252} and that in EcIDH includes ^{267}KVKLWP^{262}, and, as suggested by the numbering, they run in opposite directions. Note that residue 259 in EcIDH (not labeled) is supposed to be an aspartate, but according to the header from PDB code 5ICD, this amino acid was truncated at the β-carbon because some "side chain atoms could not be located in the electron density maps". *C*, molecular surface rendering of the active site, phosphorylation loop, and insert region (lack thereof) in phosphorylated EcIDH (6; PDB code 4ICD); recall that there is no dramatic conformational change between the dephosphorylated and phosphorylated forms of EcIDH. One monomer is *cyan*; the other is *white*. The phosphate moiety on Ser^{113} is *red*/*white* and is depicted as a van der Waals surface. *D*, molecular surface rendering of the corresponding segments in BsIDH. The subunits and modeled phosphate moiety on Ser^{104} are *colored* as they are in *C*. The phosphate is obscured both by the large indentation of the phosphorylation loop and the insert region of the opposing monomer. For clarity, the view represented in *A* and *B* has been rotated slightly toward the reader relative to that presented in *C* and *D*. *Panels C* and *D* were generated with GRASP (46).

IDH-K/P. The region of EcIDH that has been replaced in BsIDH would be a logical candidate for this docking site since it is located at the entrance to the active site cavity. BsIDH would then be a poor substrate for IDH-K/P because it lacks portions of this docking site.

These hypotheses are neither exchaustive nor mutually exclusive. It is entirely possible that all of these factors, or some combination thereof, causes BsIDH to be a poor substrate of the kinase/phosphatase. Fully discerning the reason(s) behind this observation should offer greater insight into substrate recognition of IDH-K/P for its natural substrate, EcIDH.

Acknowledgments—We thank Dr. Norma E. C. Duke and Dr. Rongguang Zhang for assistance during data collection at the Structure Biology Center-CAT of Argonne National Laboratory. We acknowledge the Minnesota Supercomputer Institute for use of computational resources and Ed Hoeffner for maintenance of x-ray instrumentation and additional computer equipment at the University of Minnesota. Finally, we thank Dr. Antony M. Dean for insightful comments regarding the manuscript, especially Fig. 7.

REFERENCES

1. Dean, A. M. and Koshland, D. E., Jr. (1993) *Biochemistry* **32,** 9302–9309
2. Kornberg, H. L. (1966) *Biochem. J.* **99,** 1–11
3. LaPorte, D. C., Walsh, K., and Koshland, D. E., Jr. (1984) *J. Biol. Chem.* **259,** 14068–14075
4. Nimmo, G. A., and Nimmo, H. G. (1984) *Eur. J. Biochem.* **141,** 409–414
5. LaPorte, D. C., Thorsness, P. E., and Koshland, D. E., Jr. (1985) *J. Biol. Chem.* **260,** 10563–10568
6. Hurley, J. H., Dean, A. M., Thorsness, P. E., Koshland, D. E., Jr., and Stroud, R. M. (1990) *J. Biol. Chem.* **265,** 3599–3602
7. Sprang, S. R., Acharya, K. R., Goldsmith, E. J., Stuart, D. I., Varvill, K., Fletterick, R. J., Madsen, N. B., and Johnson, L. N. (1988) *Nature* **336,** 215–221
8. Stroud, R. M. (1991) *Curr. Opin. Struct. Biol.* **1,** 826–835
9. Hurley, J. H., Dean, A. M., Sohl, J. L., Koshland, D. E., Jr., and Stroud, R. M. (1990) *Science* **249,** 1012–1016
10. Hurley,, J. H., Dean, A. M., Koshland, D. E., Jr., and Stroud, R. M. (1991) *Biochemistry* **30,** 8671–8678
11. Stoddard, B. L., Dean, A. M., and Koshland, D. E., Jr. (1993) *Biochemistry* **32,** 9310–9316
12. Thorsness, P. E., and Koshland, D. E., Jr. (1987) *J. Biol. Chem.* **262,** 10422–10425
13. Dean, A. M., Lee, M. H. I., and Koshland, D. E., Jr. (1989) *J. Biol. Chem.* **264,** 20482–20486
14. Dean, A. M., and Koshland, D. E., Jr. (1990) *Science* **249,** 1044–1046
15. LaPorte, D. C., and Koshland, D. E., Jr. (1982) *Nature* **300,** 458–460
16. Kemp, B. E., Graves, D. J., Benjamini, E., and Krebs, E. G. (1977) *J. Biol. Chem.* **252,** 4888–4994
17. Knighton, D. R., Zheng, J., Ten Eyck, L. F., Xuong, N.-H., Taylor, S. S., and Sowadski, J. M. (1991) *Science* **253,** 414–420
18. McKee, J. S., Hlodan, R., and Nimmo, H. G. (1989) *Biochimie (Paris)* **71,** 1059–1064
19. Miller, S. P., Chen, R., Karschnia, E. J., Romfo, C., Dean, A. M., and LaPorte, D. C. (2000) *J. Biol. Chem.* **275,** 833–839
20. Hurley, J. H., Thorsness, P. E., Ramalingham, V., Helmers, N. H., Koshland, D. E. Jr., and Stroud, R. M. (1989) *Proc. Natl. Acad. Sci. U. S. A.* **86,** 8635–8639
21. Finer-Moore, J., Tsutakawa, S. E., Cherbavaz, D. B., LaPorte, D. C., Koshland, D. E., Jr., and Stroud, R. M. (1997) *Biochemistry* **36,** 13890–13896

22. Matsuno, K., Blais, T., Serio, A. W., Conway, T., Henkin, T. M., and Sonenshein, A. L. (1999) *J. Bacteriol.* **181,** 3382–3391
23. Peterson, G. L. (1979) *Anal. Biochem.* **100,** 201–220
24. Lowry, O. H., Rosebrough, N. J., Farr, A. L., and Randall, R. J. (1951) *J. Biol. Chem.* **193,** 265–275
25. Matthews, B. W. (1968) *J. Mol. Biol.* **33,** 491–497
26. Howard, A., Gilliand, G., Finzel, B., Poulos, T., Ohlendorf, D., and Salemme, F. (1978) *J. Appl. Crystallogr.* **20,** 383–387
27. Otwinowski, Z., and Minor, W. (1997) *Methods Enzymol.* **276,** 307–326
28. Huber, R. (1965) *Acta Crystallogr. Sect. A* **19,** 353–356
29. Steigemann, W. (1974) *The Development and Use of Computational Techniques and Programs for Structural Analyses of Proteins—for Example the Trypsin-Trypsin Inhibitor Complex, the Free Inhibitor and L-Asparaginase*, Ph.D. thesis, Technische Universitaet Muenchen
30. Brünger, A. T. (1990) *X-PLOR Version 3.1: A System for Crystallography and NMR*, Yale University Press, New Haven, CT
31. Brünger, A. T. (1990) *Acta Crystallogr.* **A46,** 46–57
32. Fuginaga, M., and Read, R. J. (1987) *J. Appl. Crystallogr.* **20,** 517–521
33. Brünger, A. T., Kuriyan, J., and Karplus, M. (1987) *Science* **235,** 458–460
34. Brünger, A. T. (1992) *Nature* **355,** 472–474
35. Brünger, A. T., Krukowski, A., and Erickson, J. (1990) *Acta Crystallogr. Sect. A.* **46,** 585–593
36. Luzzati, V. (1952) *Acta Crystallogr.* **5,** 802–810
37. Jiang, J.-S., and Brunger, A. T. (1994) *J. Mol. Biol.* **243,** 100–115
38. Jones, A. T., Zou, J. Y., Cowan, S. W., and Kjeldgaard, M. (1991) *Acta Crystallogr. Sect. A* **47,** 110–119
39. Kleywegt, G. J., and Jones, T. A. (1994) in *From First Map to Final Model* (Bailey, S., Hubbard, R., and Waller, D., eds.) pp. 59–66, SERC Daresbury Laboratory, Warrington, UK
40. Kleywegt, G. J., and Jones, T. A. (1999) *Acta Crystallogr. Sect. D Biol. Crystallogr.* **55,** 941–944
41. Jones, T. A. (1992) in *Molecular Replacement* (Dodson, E. J., Gover, S., and Wolf, W., eds) pp. 91–105, SERC Daresbury Laboratory, Warrington, UK
42. Levitt, D. G., and Banaszak, L. J. (1993) *J. Appl. Crystallogr.* **26,** 736–745
43. Laskowski, R. A., MacArthur, M. W., Moss, D. S., and Thornton, J. M. (1993) *J. Appl. Crystallogr.* **26,** 283–291
44. Kleywegt, G. A., and Jones, T. A. (1994) *ESF/CCP 4 Newsletter* **31,** 9–14
45. Kaleidagraph Synergy Software. (1996) *v.* 3.5
46. Sridharan, S., Nicolls, A., and Sharp, K. (1995) *J. Comput. Chem.* **16,** 1038–1044
47. Evans, S. V. (1993) *J. Mol. Graphics* **11,** 134–138
48. Ramachandran, G., and Sasisekharan, V. (1968) *Adv. Prot. Chem.* **23,** 283–286
49. Duret, L., Gasteiger, E., and Perriere, G. (1996) *Comput. Appl. Biosci.* **12,** 507–510